

Implementation of the Generalized Complementary Flux Constraint for Low-Loss Active Magnetic Bearings

Brian C. Wilson *

Air Force Research Laboratory, Kirtland AFB, NM, 87117-5776, USA

Panagiotis Tsiotras †

Georgia Institute of Technology, Atlanta, GA 30332-0150, USA

Bonnie Heck-Ferri ‡

Georgia Institute of Technology, Atlanta, GA 30332-0250, USA

This paper explores the experimental issues associated with the implementation of the recently developed generalized complementary flux constraint (GCFC) flux-biasing scheme on a spacecraft reaction wheel that is magnetically suspended by a low-loss active magnetic bearing (AMB). Implementation of the GCFC depends fundamentally on the ability to estimate the electromagnet flux. Once addressed, other fundamental issues including the synthesis of a (possibly time-varying) bias flux and the realization of the state-dependent, voltage-switching rule that imposes the GCFC are studied. Significant filtering is required to obtain clean flux measurements and avoid spurious voltage switchings. Open-loop tests experimentally verify that the voltage-switching rule imposes the GCFC flux constraints on the operation of the electromagnets. A passivity-based control algorithm is used to illustrate the closed-loop functioning of the GCFC in large-bias and zero-bias modes of operation to demonstrate the effect of the bias flux on the closed-loop bearing stiffness, damping, and flux slew-rate.

Nomenclature

AMB active magnetic bearing
FWB flywheel battery
CMG control moment gyroscope
ESCMG energy storage control moment gyroscope
CFS constant flux sum
CFC complementary flux constraint
GCFC generalized complementary flux constraint
ZB zero-bias
LB low-bias
PMSM permanent magnet synchronous motor
IPACS integrated power and attitude control system

I. Introduction

THE frictionless operation of the active magnetic bearing (AMB) has been taken advantage of in several industrial and scientific applications including vacuum pumps, hard disk drives, high-speed centrifuges

*Electrical Engineer, Space Vehicles Directorate, 3550 Aberdeen Ave, Kirtland AFB NM, 87117-5776, AIAA Member.

†Prof. Aerospace Engineering, Georgia Institute of Technology, Atlanta, GA 30332-0150, USA, AIAA Associate Fellow.

‡Prof. Electrical Engineering, Georgia Institute of Technology, Atlanta, GA 30332-0250, USA.

and turbines, artificial heart pumps, power quality conditioning, un-interruptible power supplies, magnetic catapults, high speed milling machines, magnetically levitated trains, etc.¹⁻⁵ In such applications, control algorithms are often employed to provide functionality that other types of bearing do not possess, such as compensation for rotor imbalance and/or rotor shaft flexibility. Several practical advantages, for instance the elimination of lubrication, vacuum operation, and the non-contacting nature, allow for low-maintenance, long life-span, high-speed bearings. In spite of the long list of benefits, AMBs do have some fundamental limitations including flux saturation, resulting in limited load capacity, and force slew-rate limits.

The primary interest of the aerospace community in AMBs is their application in flywheel batteries (FWBs) and advanced control moment gyroscopes (CMGs).⁶ In a FWB, kinetic energy is stored in the rotating flywheel and converted back and forth to electrical energy using a motor/generator. FWBs have several advantages over the chemical batteries which are typically employed on spacecraft, such as long-life, large depth-of-discharge, a well-defined state-of-charge, and do not require constant or taper charging profiles.⁷ Furthermore, FWBs may be designed^a to compete with chemical batteries in terms of specific energy and typically outperform chemical batteries in terms of specific power. Advanced energy storage control moment gyroscopes (ESCMGs) that employ AMB-levitated rotors act as both a FWB and an attitude control actuator. These devices have been proposed to combine the functions of the attitude control and energy storage subsystems of satellites. Such an Integrated Power and Attitude Control System (IPACS) is projected to significantly reduce the satellite weight as well as double the mission lifespan.⁶ Furthermore, ESCMGs are viewed as an enabling technology for space missions which require large attitude control torques and high pulse-power capability, such as Space Radar.^{8,9}

Highly efficient FWBs require the use of *low-loss* AMBs. Although the use of a vacuum-operated AMB eliminates the mechanical losses in a FWB, electrical (magnetic core and Ohmic) and electromechanical (eddy-current drag) losses are often significant. Since each of these power loss mechanisms is proportional to the square of the electromagnet flux, it is imperative to minimize the flux required for rotor regulation to achieve a FWB with efficient energy storage capabilities.

Control design for an AMB is a two step process. The net force along an AMB control axis is $F = f_1 - f_2$, where f_1 and f_2 are the attractive (non-negative) forces from electromagnets 1 and 2 that compose the AMB control axis. The first step is to select an operational constraint between the electromagnets 1 and 2 so that for given a desired net force F , there exists a unique choice for f_1 and f_2 . Once the constraint is determined, a stabilizing control law is constructed.

The customary constraint is called the constant-flux-sum^b (CFS) constraint.¹⁰ Using this constraint, a large flux bias is introduced into the electromagnets and the system is linearized about this operating point. Since power dissipation is proportional to the square of the flux, AMB and FWB power losses are minimized by operating the AMB with the smallest flux bias possible, ideally zero bias (ZB). However, the CFS biasing scheme results in an uncontrollable linearization in ZB. On other words, the AMB employing the CFS is linearly uncontrollable in ZB. Thus, one must avoid the customary biasing scheme when implementing low-loss AMBs.

One solution to this fundamental, zero-bias, linear controllability limitation is to use a nonlinear control scheme where opposing electromagnets of the AMB are activated in a complementary fashion. During operation, one electromagnet is turned off while the other is on and vice versa. Under this zero-bias *complementary flux constraint* (CFC), the AMB retains nonlinear controllability, but AMB performance may be sacrificed for low-loss operation, depending on the performance measure. For instance, bearing stiffness and force slew-rate are reduced as the bias flux is decreased.

Tsiotras and Wilson¹¹ propose a *generalized complementary flux constraint* (GCFC) for low-loss AMB operation. The GCFC is an extension of the CFC flux biasing scheme that allows one to operate an AMB with a large flux bias (to obtain a desired bearing stiffness and slew-rate) or with a very small bias (for low-loss AMB operation). In fact, using the GCFC one may reduce the bias all the way to zero^c while retaining controllability, a feature that is absent from the standard CFS biasing technique. Furthermore, this bias level may be changed on-line to meet possibly time-varying performance requirements.

The low bearing stiffness implied in low-loss AMB operation introduces challenges into the control algorithm design. In particular, ZB operation leads to control law singularities when using voltage-mode

^aFlywheel batteries for spacecraft are designed to spin with maximum angular velocities on the order of 60 – 100 krpm.

^bWhen current is used to represent the electromagnet state, this constraint is called the constant-current-sum (ccs) constraint.¹⁰

^cIn this case, the GCFC corresponds to the CFC.

amplifiers and standard nonlinear control design tools such as feedback linearization and integrator backstepping.^{11–14} Typically, a control law singularity manifests itself as an infinite control voltage command. The control laws posed by Tsiotras and Wilson,¹¹ derived from the theory of dissipativity and control Lyapunov functions, effectively eliminate any singularity issues associated with voltage-mode, ZB and very low-bias (LB) operation.

The control techniques posed by Tsiotras and Wilson,¹¹ which rely on the GCFC biasing scheme, have been experimentally validated on a magnetically suspended spacecraft reaction wheel^d (illustrated in Figure 1) to evaluate their applicability in a noisy, realistic environment. Although the construction of a stabilizing control law is an important topic, the issues associated with the experimental implementation of the GCFC flux-biasing scheme are central to this presentation. Implementation of the GCFC depends fundamentally on the ability to estimate the electromagnet flux, including its DC component. To this end, a lookup table relating the flux to the current and position measurements is constructed and integrated into the AMB model. Significant filtering is required to obtain clean flux measurements. With this tool in hand, other fundamental issues including the synthesis of a (possibly time-varying) flux bias and the realization of the state-dependent, voltage-switching rule that imposes the GCFC are studied. Specifically, the implementability of the GCFC method is experimentally validated on the PREMAG reaction wheel. Furthermore, as a means to illustrate the closed-loop functioning of the GCFC in large-bias and ZB modes of operation, a passivity-based control law¹¹ is employed to stabilize the rotor. The effects of the bias level on the closed-loop bearing stiffness, damping, and force slew-rate are discussed. To motivate ZB and LB AMB operation, this study begins with an energy analysis of the AMB and FWB to illuminate the source of the power dissipation mechanisms.

II. Dynamics and Energy Analysis of the FWB and the 1-DOF AMB

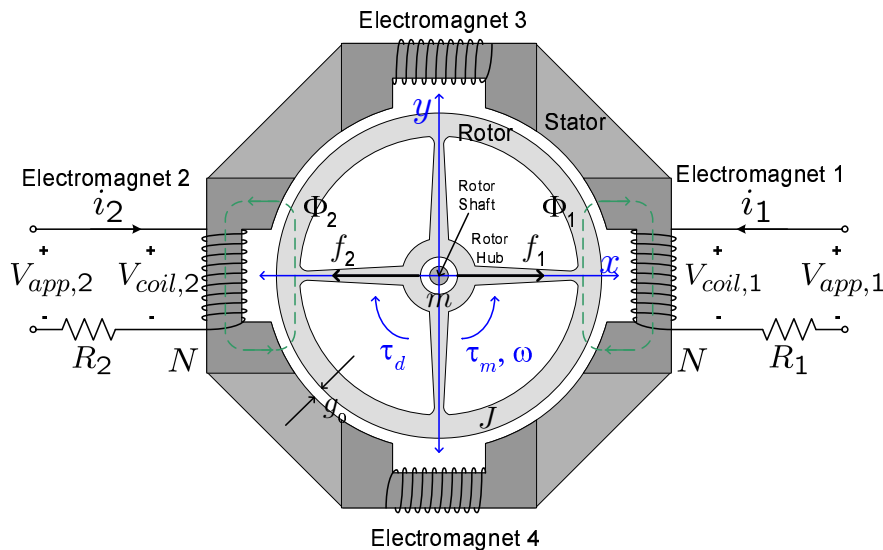


Figure 1. A two-dimensional schematic of the PREMAG magnetically suspended reaction wheel.

A two-dimensional schematic of the flywheel battery used in this investigation is shown in Figure 1. The rotor is regulated in the $x - y$ plane by electromagnets 1 through 4. When the rotor is centered in the $x - y$ plane the nominal airgap between the rotor and stator is g_0 . Although omitted from the above schematic for clarity, four additional electromagnets, located directly beneath electromagnets 1 through 4, allow for control of the rotor tilt about the x and y axes. Although the full 6-DOF rotor control problem is worthy of study, this work ignores the rotor gyroscopic effects and instead focuses on the simpler control problem which assumes that four independent controllers can be designed to regulate the translational motion of the top and bottom of the rotor in the $x - y$ plane. Therefore, only the implementation of the GCFC on one of the AMB control axes is presented. A passive bearing supports the rotor's weight in the z direction (out

^dNote that this device was originally constructed by PREMAG Magnetic Bearings Inc. as a 6-DOF magnetically suspended reaction wheel for use in a small satellite. It has been modified to act as a control design test bed for low-loss AMBs.

of the page) and is omitted in this discussion. In this particular FWB configuration, the spin torque about the z axis is generated from a permanent magnet synchronous motor (PMSM) that is integrated into the interior of the rotor hub.

A. The FWB and 1-DOF AMB Model

The flywheel rotational dynamics are

$$J\dot{\omega} = \tau_m - \tau_d, \quad (1)$$

where J is the rotor rotational inertia about the spin axis, ω is the rotor angular velocity, τ_m is the torque applied by the spin motor, and τ_d is the electromagnetic drag torque. For $\omega \geq 0$, the PMSM acts as a motor when $\tau_m \geq 0$ and as a generator when $\tau_m < 0$. The electromagnetic drag torque, which results from eddy-current induction in the surface of the rotor, always opposes the rotor angular velocity and is^{15–17}

$$\tau_d = pG\Phi^2\omega = k_d\omega, \quad (2)$$

where p is the number of electromagnets, G is a constant that depends on the AMB geometry and material properties, and Φ is the electromagnet flux. The drag coefficient k_d may be experimentally identified through rotor spin-down tests with $\tau_m = 0$.

Since the ratio of rotor radius r to the nominal airgap g_0 is large, the customary “small airgap” assumption is made. Consequently, the electromagnet forces in the x and y direction are decoupled. Henceforth, only the x -axis, 1-DOF AMB dynamics are considered. The translational equation of motion is

$$m\ddot{x} = F = f_1 - f_2, \quad (3)$$

where m is the rotor mass, f_1 and f_2 are the electromagnet forces as illustrated in Figure 1, and F is the total electromagnet force on the rotor in the x direction. The force from each electromagnet is^{16,18}

$$f_j = \frac{\Phi_j^2}{\mu_0 A_g}, \quad j = 1, 2 \quad (4)$$

where Φ is the electromagnet flux, μ_0 is the permeability of free space, and A_g is the cross-sectional area of the airgap. Generally, the flux Φ is a nonlinear, multi-valued hysteresis function of the electromagnet current and the airgap: $\Phi = h(i, x)$. Under some mild presumptions, a technique exists for approximating this function using a lookup table: See the discussion in Section IV-A. The function $h(i, x)$ that is produced from this approximation technique may be viewed as a flux estimator, valid for reconstruction of the flux from DC up to some bandwidth, in terms of the readily available position and current measurements. Using this technique, the effects of AMB flux saturation are incorporated into the model of $h(i, x)$, a property that other force-current-position relationships often neglect.

The electromagnet coils in Figure 1 are represented by zero-resistance coils (i.e. ideal coils) and a resistor R to account for the distributed winding resistance. Faraday’s law relates the rate of change of coil flux to the voltage across the ideal coil: $N\dot{\Phi} = V_{\text{coil}}$. Kirchhoff’s voltage law relates the ideal coil voltage to the terminal coil voltage V_{app} . Using these principles, the resulting electrical dynamics are

$$\begin{aligned} V_{\text{app},j} &= i_j R + V_{\text{coil},j} \\ &= i_j R + N\dot{\Phi}_j, \quad j = 1, 2 \end{aligned} \quad (5)$$

where i is the coil current. In this study, voltage-mode amplifiers are used to drive the electromagnet coils.

Remark 1. (*current-mode vs. voltage-mode amplifiers*)

Electromagnet coils are typically driven by power servo amplifiers configured to operate in current mode or voltage mode. In current mode, feedback internal to the servo amplifier is used to make the coil current track a reference current. In voltage mode, feedback internal to the servo amplifier is used to make the voltage V_{app} in equation (5) track a reference voltage V_r . The transfer function of V_{app}/V_r typically resembles a low-pass filter with several hundred Hertz bandwidth.

B. Energy and Loss Analysis of the FWB and 1-DOF AMB

Energy is stored in the flywheel battery in the form of kinetic energy, $\mathcal{K} = \frac{1}{2}J\omega^2$. Using $\dot{\mathcal{K}} = J\omega\dot{\omega}$ and the flywheel equation of motion (1), the FWB energy storage dynamics are

$$\begin{aligned}\dot{\mathcal{K}} &= J\dot{\omega}\omega = \tau_m\omega - \tau_d\omega \\ &= \tau_m\omega - k_d\omega^2 \\ &= \tau_m\omega - \tilde{k}_d\frac{J}{2}\omega^2 \\ &= -\tilde{k}_d\mathcal{K} + \tau_m\omega,\end{aligned}\tag{6}$$

where $\tilde{k}_d = 2k_d/J$. Without loss of generality, the angular velocity is assumed to be non-negative. When acting as a motor, the electrical energy at the input terminals of the PMSM is converted to mechanical power, $\tau_m\omega$ is positive, and the mechanical energy stored in the flywheel increases. When acting as a generator, mechanical energy stored in the flywheel is converted to electrical power available at the PMSM's terminals, $\tau_m\omega$ is negative, and the mechanical energy stored in the flywheel decreases. The electromagnetic drag torque introduces a stable, first order pole into the energy storage dynamics. Thus, even when drawing no electrical power in generator mode ($\tau_m = 0$) from the flywheel, the ‘‘charge’’ stored in the flywheel battery will exponentially decay to zero with time constant $1/k_d$. Ideally, if $k_d = 0$, the energy storage dynamics are lossless and all of the input power is stored indefinitely in the FWB. Assuming that k_d is proportional to Φ_0^2 (see Remark (2)) it is imperative to minimize Φ_0 in the control design, ideally to zero, to maximize the FWB energy storage efficiency.

In addition to electromagnetic drag losses in the FWB, there are losses associated with the operation of the electromagnets. Energy conversion from the AMB electrical input power to the mechanical force that produces rotor translation takes place in the magnetic field of the AMB coil. The dynamics of the magnetic field energy storage along the x control axis are^{16, 18}

$$\dot{E}_{\text{fld},j} = -f_j\dot{x}_j + V_{\text{app},j}i_j - i_j^2R - p_{\text{core},j}, \quad j = 1, 2\tag{7}$$

where E_{fld} is the energy stored in the electromagnet magnetic field, $f\dot{x}$ is the translational mechanical output power, $V_{\text{app}}i$ is the electrical input power, i^2R is the Ohmic loss, and p_{core} represents the losses in the electromagnetic core due to eddy-current generation and hysteresis. Observe that the electrical input power $V_{\text{app}}i$ increases the stored magnetic energy and the mechanical output power $f\dot{x}$, Ohmic loss i^2R , and core loss p_{core} decrease the stored magnetic energy. The AMB Ohmic and core loss are proportional to Φ^2 . An efficient AMB has minimal Ohmic and core losses so that the fraction of the electrical input power delivered to the AMB that is converted into useful mechanical output power is maximized.

Table 1. Summary of FWB and AMB power losses.^{16, 18, 19}

Power Loss	Proportional to
Ohmic loss in coil	$\propto \Phi^2, i^2R$
eddy-current loss in core	$\propto \Phi_{\text{max}}^2$
hysteresis loss in core	$\propto \Phi_{\text{max}}^{1.5-2.5}$
eddy-current drag loss	$\propto p, \Phi^2, \omega^2$

Remark 2. (Low-Loss FWB and AMB operation)

The FWB and AMB power loss mechanisms are summarized in Table 1. The instantaneous power loss in each mechanism is proportional to the square of the magnetic flux. Since the flux is time-varying, one may minimize the rms power losses in both the FWB and the AMB by minimizing the rms value of the flux required to operate the AMB. When employing control designs that introduce a flux bias— for example, let $\Phi_j = \Phi_0 + \phi_j$ where Φ_j is the total electromagnet flux, Φ_0 is the constant flux bias, and ϕ_j is the control flux in the j^{th} electromagnet – the flux bias Φ_0 should be minimized to reduce the wasteful energy dissipation in the AMB and FWB.

III. AMB Flux Biasing and Performance Measures

Integral to every AMB control design is the selection of an operating constraint between the electromagnets that compose an AMB control axis. Since the total force along the x -axis, for example, is $F = f_1 - f_2$, there exist an infinite number of non-negative (electromagnet forces are always attractive) choices of f_1 and f_2 to realize a given desired total force F_{des} . Thus, the AMB designer must supply a constraint equation between f_1 and f_2 to uniquely determine f_1 and f_2 for a given total force, F_{des} . Typically, these force constraints are indirectly imposed through a constraint applied to the electromagnet voltage, current, or flux.¹⁰ To illustrate the limitations of the standard biasing scheme for use with low-loss AMBs, the constant-flux-sum (CFS) constraint is first discussed. Next the generalized complementary flux constraint (GCFC) and the voltage switching law that implements it are introduced. Section III-C discusses the effect of the bias level on AMB performance measures such as, static load capacity, force slew-rate, closed-loop bearing stiffness and damping.

A. The Constant-Flux-Sum (CFS) Constraint

This constraint introduces a constant flux bias Φ_0 into the electromagnets so that $\Phi_1 = \Phi_0 + \phi_1$ and $\Phi_2 = \Phi_0 + \phi_2$. Since the electromagnet force depends on the square of the flux, the sign of the flux is immaterial. However, the fluxes are implemented so that Φ_1 and Φ_2 are always non-negative. The CFS constraint is imposed so that the sum of the total fluxes at all times is constant: $\Phi_1 + \Phi_2 = 2\Phi_0$. This implies that $\phi_1 = -\phi_2$. Conveniently, the two control fluxes ϕ_1 and ϕ_2 reduce to one by defining $\phi = \phi_1 = -\phi_2$. The control flux ϕ produces a net force in a differential manner:

$$\Phi_1 = \Phi_0 + \phi \quad (8a)$$

$$\Phi_2 = \Phi_0 - \phi, \quad (8b)$$

with the corollary constraint $|\phi| \leq \Phi_0$ so that Φ_j is non-negative for $j = 1, 2$.

The main advantage of the CFS is that it exactly linearizes the AMB translational dynamics permitting implementation of simple linear control algorithms in terms of ϕ as the control input. Imposing (8) on the translational equation of motion (3), one obtains

$$\begin{aligned} m\ddot{x} = F &= \frac{1}{\mu_0 A_g} [\Phi_1^2 - \Phi_2^2] \\ &= \frac{1}{\mu_0 A_g} [(\Phi_0 + \phi)^2 - (\Phi_0 - \phi)^2] \\ &= \frac{4\Phi_0}{\mu_0 A_g} \phi, \quad |\phi| < \Phi_0. \end{aligned} \quad (9)$$

Since low-loss operation is desirable, Φ_0 should be reduced ideally to zero. However, as Φ_0 tends towards zero in equation (9), the total electromagnet force becomes zero resulting in an uncontrollable system. Thus, the main advantage of the CFS technique, namely the exact linearization property, is nullified by the absence of linear controllability under low-loss conditions. Consequently, the CFS constraint is a poor design choice for low-loss AMB operation.

B. Complementary Flux Constraints

The generalized complementary flux condition (GCFC) also introduces a flux bias ($\Phi_j = \Phi_0 + \phi_j$, $j = 1, 2$), however, the control fluxes are constrained such that $\phi_1 \phi_2 = 0$. Thus, at any given time, one of the control fluxes is zero while the other is adding to the bias flux to create a net force. For convenience, introduce the *generalized control flux*

$$\phi := \phi_1 - \phi_2. \quad (10)$$

The GCFC constraint written in terms of ϕ is

$$\begin{aligned} \phi_1 = \phi, \quad \phi_2 = 0 & \quad \text{when} \quad \phi \geq 0 \\ \phi_1 = 0, \quad \phi_2 = -\phi & \quad \text{when} \quad \phi < 0, \end{aligned} \quad (11)$$

and is imposed by following voltage-switching rule¹¹

$$\begin{aligned} V_{c1} &= v, & V_{c2} &= 0 & \text{when } \phi &\geq 0 \\ V_{c1} &= 0, & V_{c2} &= -v & \text{when } \phi < 0, \end{aligned} \quad (12)$$

where V_{c_j} are the voltage reference inputs to the voltage-mode amplifiers and v is the *generalized control voltage* such that the electrical dynamics of equation (5) reduce to

$$\dot{\phi} = \frac{v}{N}. \quad (13)$$

For simplicity, the resistance has been neglected. Alternatively, one may redefine the control input by letting $v = V_{\text{app}} - iR$ to cancel the resistance.

Imposing this flux constraint on the translational dynamics, (3) one obtains

$$\begin{aligned} m\ddot{x} &= F = \frac{1}{\mu_0 A_g} (\Phi_1^2 - \Phi_2^2) \\ &= \frac{1}{\mu_0 A_g} [\phi_1^2 - \phi_2^2 + 2\Phi_0(\phi_1 - \phi_2)] \\ &= \frac{1}{\mu_0 A_g} (2\Phi_0\phi + \phi|\phi). \end{aligned} \quad (14)$$

Due to the presence of the $\phi|\phi$ term in equation (14), the AMB retains its controllability properties as Φ_0 reduces to zero. In this case, the control fluxes are equal to the total fluxes $\phi_j = \Phi_j$ for $j = 1, 2$, and the generalized control flux is $\phi = \Phi_1 - \Phi_2$. Consequently, the GCFC implements the standard CFC (see Ref. [11]) as a special case when the flux bias is zero.

C. AMB Performance Measures

Closed-loop AMB performance^{20,21} is often characterized in terms of static load capacity, bearing stiffness, and force slew-rate. Such characterizations, which arise from the field of rotordynamics,⁷ facilitate an analogy where the AMB-levitated rotor under closed-loop control behaves similarly to a rotor on conventional bearings with a given spring stiffness and damping.

The AMB static load capacity is a measure of the peak force that the bearing can produce. For any electromagnet, the maximum force is given by $F_{\text{max}} = \Phi_{\text{sat}}^2 / \mu_0 A_g$, where Φ_{sat} is the value of the flux that saturates the electromagnet core. This is determined by the saturation flux density B_{sat} of the electromagnetic core material^e and the cross-sectional area A_p of the electromagnet pole: $\Phi_{\text{sat}} = B_{\text{sat}} A_p$. When employing the GCFC constraint, the AMB static load capacity is limited only by the saturation flux density. Thus, the GCFC static load capacity is $F_{\text{GCFC}} = F_{\text{max}}$. On the other hand, the largest force that the CFS constrained AMB can produce is $F_{\text{CFS}} = (2\Phi_0)^2 / \mu_0 A_g$. Consequently, if $\Phi_0 < \Phi_{\text{sat}}/2$, then $F_{\text{CFS}} < F_{\text{max}}$. In this case, the CFS scheme artificially limits the static load capacity of the AMB to less than the capacity of the electromagnets.

The force slew-rate measures the rate-of-change of the force with time. The time derivative of the force using equation (13) is

$$\dot{F}(\phi) = \frac{dF}{d\phi} \dot{\phi} = \frac{dF}{d\phi} \frac{v}{N} \leq \frac{dF}{d\phi} \frac{V_s}{N} \quad (15)$$

where the control voltage is assumed to be less than the amplifier supply voltage: $v \leq V_s$. This measure is related to the amplifier bandwidth.

Closed-loop bearing stiffness and damping measure the rate-of-change of the force with respect to the rotor position and velocity, respectively. These concepts are illuminated by assuming that the control flux is designed with position and velocity feedback: $\phi = \phi(x, \dot{x})$. Using the Taylor series expansion on the net force in the resulting closed-loop equation of motion, $m\ddot{x} = F(\phi(x, \dot{x}))$, gives

$$\begin{aligned} m\ddot{x} &\approx \frac{dF}{dx} \tilde{x} + \frac{dF}{d\dot{x}} \dot{\tilde{x}} \\ &= \frac{dF}{d\phi} \frac{d\phi}{dx} \tilde{x} + \frac{dF}{d\phi} \frac{d\phi}{d\dot{x}} \dot{\tilde{x}} \\ &= K(\phi) \tilde{x} + D(\phi) \dot{\tilde{x}} \end{aligned} \quad (16)$$

^eFor common electromagnet core materials, $B_{\text{sat}} \in [0.6 - 2.0]$ Tesla.

where the tilde is used to represent the deviation from the expansion point. One identifies the possibly nonlinear stiffness $K(\phi)$ and damping $D(\phi)$ terms from equation (16).

It is clear from equation (15) and (16) that the force slew-rate, the bearing stiffness, and damping each depend on the slope of the force-flux characteristic, $\frac{dF}{d\phi}$. Equations (9) and (14) show that $\frac{d}{d\phi}F_{\text{CFS}} = 4\Phi_0/(\mu_0 A_g)$ and $\frac{d}{d\phi}F_{\text{GCFC}} = 2(\Phi_0 + |\phi|)/(\mu_0 A_g)$ are linearly proportional to the bias flux. Thus, in both the CFS and GCFC schemes, a large bias flux enhances the bearing stiffness and force slew-rate. In addition, as the bias approaches zero, the bearing stiffness and force slew-rate decrease in both CFS and GCFC schemes, however, the CFS becomes uncontrollable while the GCFC maintains nonlinear controllability.

Heuristically, one expects a bearing with a large force slew-rate and bearing stiffness to be more “responsive” and have better disturbance rejection capabilities. The low-loss AMB has opposing performance measures: a LB design is desirable for efficient FWB energy storage and AMB operation, however, at the expense of decreased bearing stiffness, damping, and force slew-rate. Depending on the requirements of the application, this trade-off may or may not be debilitating. For example, terrestrial or ground vehicle energy storage applications may need to float the FWB rotor in the presence of large external disturbances and thus require large bearing stiffness. In a satellite attitude control application on the other hand, the rotor imbalance of the ESCMG itself may be a major source of attitude pointing error. In this case, it may be beneficial to have a low bearing stiffness to reduce the transmission of the rotor imbalance to the spacecraft and its sensing instruments. Thus, understanding of the effect of the bias level on the energy storage efficiency and the controller performance (with respect to the application requirements) is an important issue when using the GCFC.

IV. GCFC Implementation

Implementation of the GCFC depends fundamentally on the ability to estimate the electromagnet flux, including its DC component. To this end, a lookup table relating the flux to the current and position measurements is constructed and integrated into the AMB model. Significant filtering is required to obtain clean flux measurements. With this tool in hand, other fundamental issues including the synthesis of a (possibly time-varying) bias flux and the realization of the state-dependent, voltage-switching rule that imposes the GCFC are discussed.

Figure 2 shows the GCFC and control law implementation block diagram for the x control axis of the PREMAG reaction wheel. The electromagnet coils are driven by Copley Controls model 412 PWM voltage-mode servo-amplifiers. The amplifiers force the electromagnet terminal voltage $V_{\text{app},j}$ to follow the reference voltage $V_{r,j}$ for $j = 1, 2$. The transfer function of $V_{\text{app},j}/V_r$ is a low-pass filter with a 200 Hz bandwidth. Since the electromagnet coils are linear in the voltage input, one may use superposition to independently realize a bias flux and control flux. To this end, each reference voltage $V_{r,j}$ is decomposed into a component that implements the flux bias $V_{b,j}$ and a component that implements the control law $V_{c,j}$:

$$V_{r,j} = V_{b,j} + V_{c,j}, \quad j = 1, 2 \quad (17)$$

The filtered current and position measurements are passed through the flux-lookup tables to produce estimates for Φ_1 and Φ_2 . Subtracting these signals gives the generalized control flux ϕ . Given Φ_1 , Φ_2 , and ϕ , one can adjust $V_{b,j}$ to drive the DC component of Φ_1 and Φ_2 to a desired flux bias level $\Phi_{0,\text{des}}$. The nonlinear control law is constructed to stabilize equations (13) and (14) with the states x , \dot{x} , and ϕ . The control voltage v produced by the controller is distributed to the proper electromagnet $V_{c,j}$ through the GCFC voltage switching rule of equation (12). Each of the blocks in Figure 2 is discussed in more detail below.

A. Flux Estimation

Several techniques exist for estimating the electromagnet flux. Direct measurement of the flux, including the DC component, is possible with Hall-effect sensors. However, since these sensors are typically too large, fragile, and expensive to integrate into an AMB, this approach is impractical. One may construct a mathematical observer²² to reconstruct the flux, however, a more direct approach is pursued here.

An auxiliary coil, called a search coil, may be employed to estimate the flux. Based on Faraday’s law ($\dot{\varphi} = V_{oc}$), this method integrates the open-circuit voltage V_{oc} of the search to obtain the flux φ . Observe that this technique fails to reconstruct the DC component of the flux because $\dot{\varphi} = V_{oc} \equiv 0$ for a constant flux

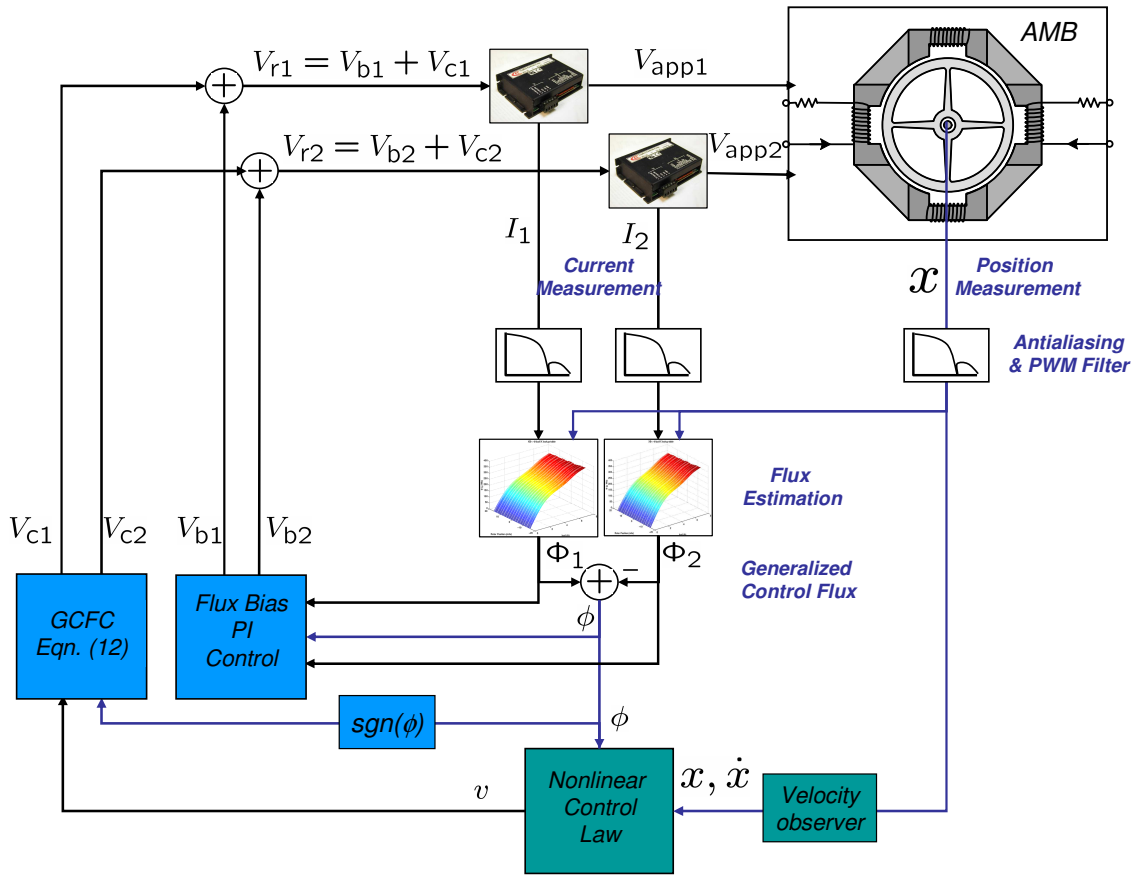


Figure 2. Block diagram of the implementation of the GCFC constraint and the control law.

signal. Thus, a search coil is only useful to reconstruct the AC portion of the flux. Nonetheless, as shown in Figure 3a, one may use AC flux data to construct a $\varphi - I$ hysteresis curve using the following procedure: (1) fix the rotor position, (2) drive the coil with a sinusoidal current (using the amplifier in current mode), (3) integrate the open-circuit voltage of the search coil to get the flux, and (4) plot the resulting $\varphi - I$ curve. The area enclosed by the hysteresis curve is related to the core losses of the material and is proportional to the excitation frequency of the current. As the excitation frequency is reduced, the hysteresis curve collapses to the DC magnetization curve. Thus, one may characterize the DC behavior of the electromagnet by fitting a DC magnetization curve to the measured AC data. A lookup table is constructed by repeating this experiment for several values of the rotor position.

Figure 3b shows the configuration of the electromagnet and the auxiliary search coil. The electromagnet coil behaves according to the equation $V_{\text{coil}} = N_c \dot{\varphi}$ and the search coil behaves according to the equation $V_s = N_s \dot{\varphi}$. Since the flux is common to both coils, $V_{\text{coil}} = \frac{N_c}{N_s} V_s$ and the electromagnet flux is given by

$$\varphi(t) = \frac{N_c}{N_s} \int_0^t V_s(\tau) d\tau \quad (18)$$

where V_s is obtained through the instrumentation amplifier shown in Figure 3b. Since the instrumentation amplifier is bound to have a DC offset and the voltage signal may contain noise with a non-zero rms value, the following transfer function is used to implement the integration:

$$\varphi(s) = \frac{N_c (1+a)s}{N_s (s+a)^2} V_s(s). \quad (19)$$

This transfer function approximates the integrator down to 50 mHz, using $a = 2\pi(50 \times 10^{-3})$, and has zero DC gain to reject the voltage offset of the instrumentation amplifier.

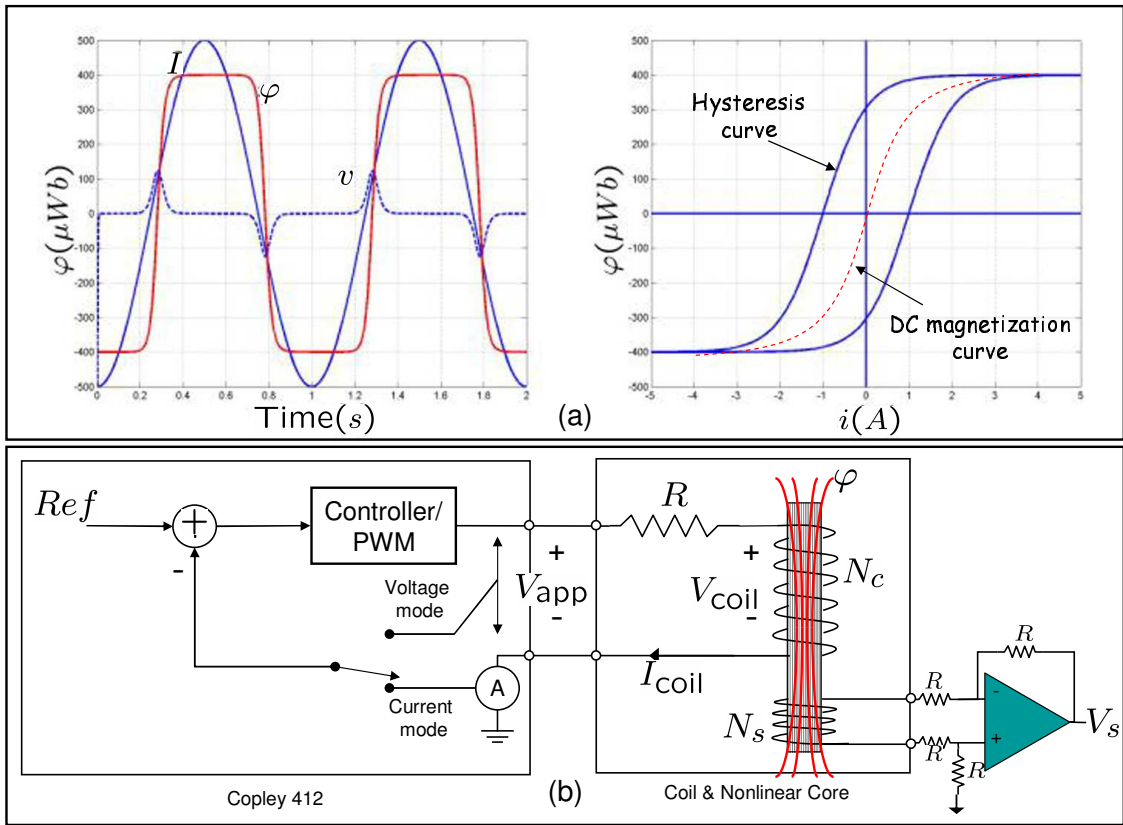


Figure 3. Flux Measurement: (a) forcing current, measured coil voltage, integrated flux, and resulting $\Phi - I$ curve. (b) Copley amplifiers and search coil setup.

Figure 4 illustrates the construction of a flux-lookup table. Figure 4a shows the forcing current, the measured open-circuit voltage, and the flux resulting from integration via equation (19). Figure 4b shows the resulting $\phi - I$ hysteresis curve and the polynomial approximation to the DC magnetization curve. Figure 4c shows the variation in the DC magnetization curve with airgap and Figure 4d shows the resulting flux-lookup table $\Phi = h(i, x)$.

B. Noise Sources and Filtering

The experiment is implemented using a dSPACE[®] DS1103 controller board sampling at 6 – 7 kHz and the accompanying MathWorks[®] and dSPACE[®] software: Matlab[®], Simulink[®], Real-Time Workshop[®], and ControlDesk[®]. The closed-loop controller bandwidths are on the order of 100 Hz. A fourth-order Sallen-Key low-pass filter, as shown in Figure 5, is designed with corner frequency at 750 Hz. This places the 3 dB bandwidth of the measured signals (currents and rotor position) well above the closed-loop controller bandwidth. Since the phase lag of the anti-aliasing filter is less than 10° for frequencies less than 100 Hz, one expects only minor degradation of the phase margin of the control law. In addition, since the 750 Hz sensor bandwidth is about $1/10^{th}$ the sampling rate, one should comfortably expect to avoid aliasing.

Aside from aliasing, the main noise source in this experiment is the PWM switching frequency of the amplifiers at 25 kHz. This noise is prominent in the current signals and couples into the position measurements. In the GCFC constraint, the control voltage v is distributed to the proper electromagnet according to the sign of the generalized control flux ϕ : See equation (12). This implies that clean flux measurements are required to avoid spurious switching of the control voltage. A twin-T notch filter, as shown in Figure 5, is used to reject the 25 kHz switching frequency. In addition to the filtering, standard noise reduction techniques are employed including twisted-shielded pair cabling, star-point grounding, and capacitive power supply bypassing.

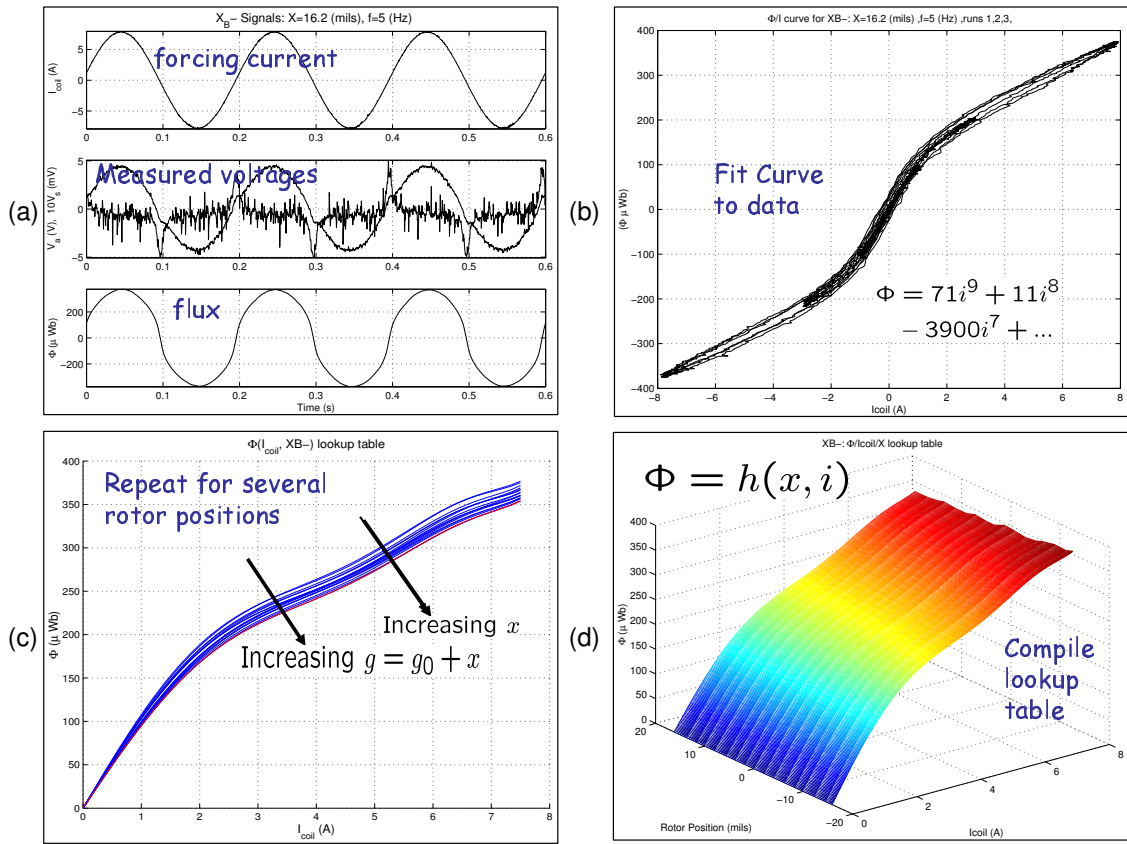


Figure 4. Lookup table construction: (a) measure flux with search coil (b) plot $\Phi - I$ curve and fit DC magnetization curve AC data (c) repeat steps a and b for several rotor positions (d) compile DC magnetization curves into lookup table

C. Flux Bias Implementation

In general, the flux depends on the current and the airgap. Therefore, feedback, which modulates the current, is required to realize a constant flux in the presence of a changing airgap. Using voltage-mode amplifiers, the bias flux is implemented by controlling the bias component $V_{b,j}$ of the amplifier reference voltage $V_{r,j}$, for $j = 1, 2$: See equation (17). Using a simple PI control law, one may drive the DC component of the electromagnet flux Φ_j to a desired bias-flux value $\Phi_{0,des}$. To clarify, let the electromagnet flux be

$$\Phi_1(t) = \Phi_{1,DC}(t) + \phi_1(t) \quad (20a)$$

$$\Phi_2(t) = \Phi_{2,DC}(t) + \phi_2(t) \quad (20b)$$

where $\Phi_{j,DC}(t)$ is the DC component of Φ_j for $j = 1, 2$ and may vary with time in general. The goal is to select $V_{b,j}$ to drive $\Phi_{j,DC}(t)$ to $\Phi_{0,des}$. To this end, use the PI control law

$$V_{b,j}(s) = (k_p + \frac{k_i}{s})e_{b,j}, \quad j = 1, 2 \quad (21)$$

with positive proportional and integral gains $k_p > 0$, $k_i > 0$, that acts on the bias error

$$\begin{aligned} e_{b,j}(t) &= \Phi_{0,des} - \Phi_{j,DC}(t), \quad j = 1, 2 \\ &= \Phi_{0,des} - \Phi_j(t) + \phi_j(t) \end{aligned} \quad (22)$$

To implement equation (22), the bias error must be measurable. Since $\Phi_{0,des}$ is set by the user, $\Phi_j(t)$ is directly measurable from the flux-lookup tables, $\phi(t) = \Phi_1(t) - \Phi_2(t)$, and the $\phi_j(t)$ are just the positive and negative complements of $\phi(t)$, equation (22) is indeed implementable and one may implement a bias flux using equation (21). Since a PI control law is used, the DC component of the flux Φ_j is able to track step changes in $\Phi_{0,des}$.

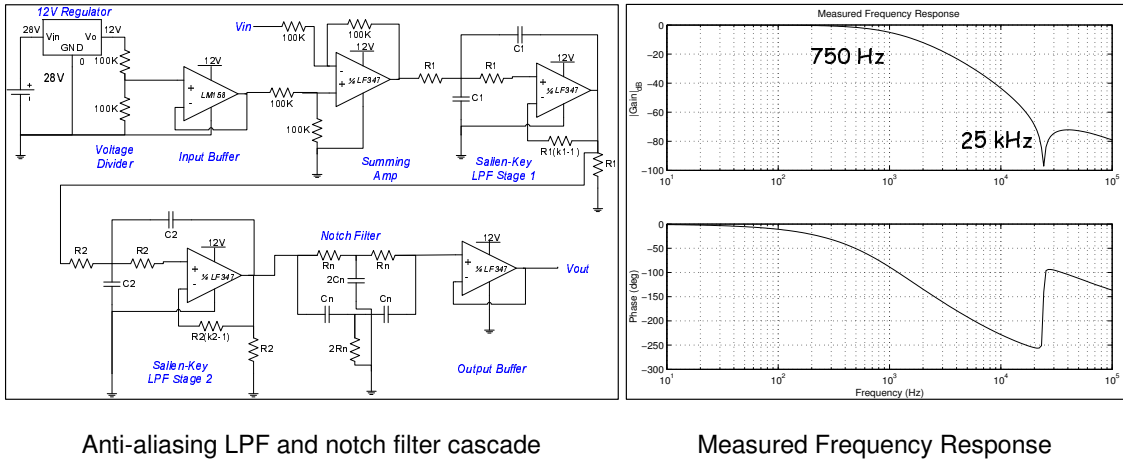


Figure 5. Anti-aliasing low-pass and PWM filter: Fourth order Sallen-Key low-pass filter with 750 Hz bandwidth cascaded with a 25 kHz twin-T notch filter.

D. Experimental Validation of the GCFC

To validate the implementation of the GCFC in the simplest manner, disconnect the control law in Figure 2 and replace the control voltage v with a sinusoidal input. Figure 6 shows the experimental implementation of the GCFC under these open-loop conditions while requesting a flux bias $\Phi_{0,\text{des}} = 100 \mu\text{Wb}$. The sinusoidal control voltage v is shown in the upper-left. This voltage is distributed to the electromagnets $V_{c,j}$ for $j = 1, 2$ according to the $\text{sgn}(\phi)$. Control voltage $V_{c,j}$ in conjunction with the bias voltage $V_{b,j}$ (omitted for clarity) produce currents i_j for $j = 1, 2$. The fluxes are calculated from the flux-lookup tables ($\Phi_j = h_j(x, i_j)$), the (uncontrolled) position x , and the currents i_j , for $j = 1, 2$. One may verify that the fluxes are complementary in the sense of equation (11) and ride on top of a $100 \mu\text{Wb}$ flux bias. One may further verify that the generalized control flux $\phi = \Phi_1 - \Phi_2$ and that $\dot{\phi} = \frac{v}{N}$ is satisfied for $N = 60$. Figure 7 shows an identical situation except that $\Phi_{0,\text{des}} = 0 \mu\text{Wb}$. In this case, the GCFC implements the CFC.

To illustrate the closed-loop functioning of the GCFC, a passivity-based control law, taken from Ref. [11,17], is used to stabilize the rotor. In order to work with a system having the minimum number of parameters, it is convenient to introduce the following non-dimensionalized state and control variables along with a non-dimensionalized time

$$\begin{aligned}
 x_1 &:= \frac{x}{g_0}, & x_2 &:= \frac{\dot{x}}{\Phi_{\text{sat}} \sqrt{g_0/\kappa}}, & x_3 &:= \frac{\phi}{\Phi_{\text{sat}}}, \\
 u &:= \frac{v \sqrt{g_0 \kappa}}{N \Phi_{\text{sat}}^2}, & \tau &:= t \frac{\Phi_{\text{sat}}}{\sqrt{g_0 \kappa}}
 \end{aligned} \tag{23}$$

where $\kappa := m\mu_0 A_g$ and Φ_{sat} is the value of the saturation flux.

In terms of these non-dimensionalized variables, the gcfc constrained dynamics (14)-(13) can be written in state-space form as follows

$$x'_1 = x_2 \tag{24a}$$

$$x'_2 = \epsilon x_3 + x_3 |x_3| := f_2(x_3) \tag{24b}$$

$$x'_3 = u \tag{24c}$$

where $\epsilon := 2\Phi_0/\Phi_{\text{sat}}$ and where prime denotes differentiation with respect to τ . Low-bias operation in this context therefore implies that $\epsilon \ll 1$, while zero bias implies that $\epsilon = 0$. The control law is computed for this system and re-dimensionalized before being applied to system (14)-(13). The passivity based control law is stated without proof in the following proposition: See [11,17] for further discussion.

Proposition 1. (Passivity-based control [11,17])

The system (24) with the control law

$$u = -k_1 z_2 - k_2 f_2(x_3) - z_2 \pi(z, x_3) - \gamma \eta \tag{25}$$

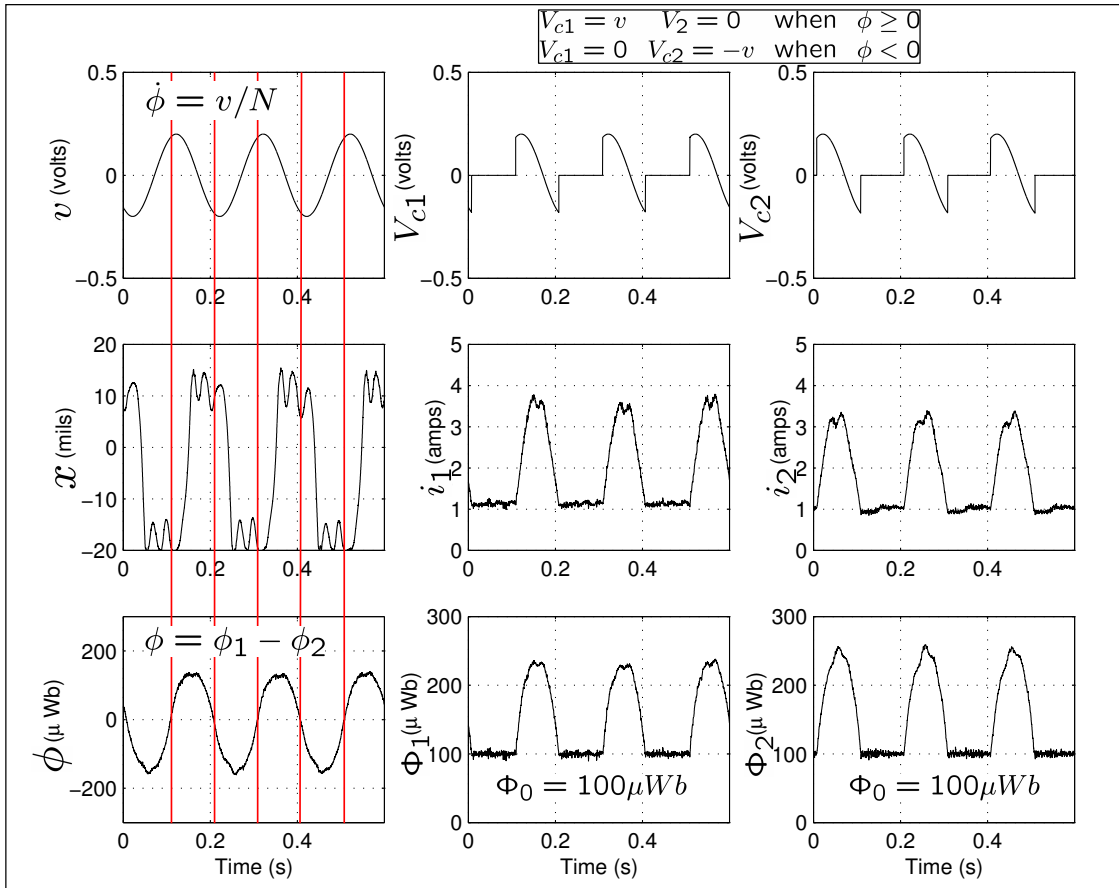


Figure 6. Open-loop GCFC implementation with sinusoidal control voltage v : $\Phi_0 = 100\mu\text{Wb}$.

where k_1, k_2, γ are positive constants, $\eta = x_3 - u_0(z)$, $u_0(z) = -k_1x_1 - k_2x_2$, and the continuous function

$$\pi(z, x_3) := \frac{f_2(x_3) - f_2(u_0(z))}{x_3 - u_0(z)}, \quad (26)$$

is globally asymptotically stable (GAS).

Figure 8 illustrates the closed-loop GCFC implementation employing the passivity-based control law of Proposition 1 with gains $k_1 = 3$, $k_2 = 0.5$, and $\gamma = 0.5$ to regulate the rotor against a periodic disturbance while implementing a bias flux $\Phi_0 = 100\mu\text{Wb}$. The rotor is regulated within an rms error of 1.4 mils to the desired set point. One may verify that the GCFC is properly implemented.

Figure 9 shows the effect of the bias value on the step response of the rotor using the passivity-based control law of Proposition 1 with gains $k_1 = 3$, $k_2 = 0.5$, and $\gamma = 0.5$. The position, control flux, and voltage are illustrated for ZB operation (left column) and large-bias ($\Phi_0 = 150\mu\text{Wb}$) operation. ZB operation results in a step response with ringing; a response typical of a bearing with little bearing stiffness and damping. On the other hand, the large bias results in fast response with no ringing; a response typical of a bearing with significant bearing stiffness and damping. Thus, when holding the control gains constant, the bias directly effects the bearing stiffness and damping as predicted in Section III-C.

V. Conclusion

Control design for the AMB is a two step process: first, a constraint must be designed (which typically implements a bias flux) so that the generation of the net electromagnet force is well-defined. Next, a stabilizing control law is constructed. Since the power loss mechanisms for the FWB and AMB are proportional to the bias flux employed in step 1, it is imperative to minimize the bias flux to realize an FWB with efficient

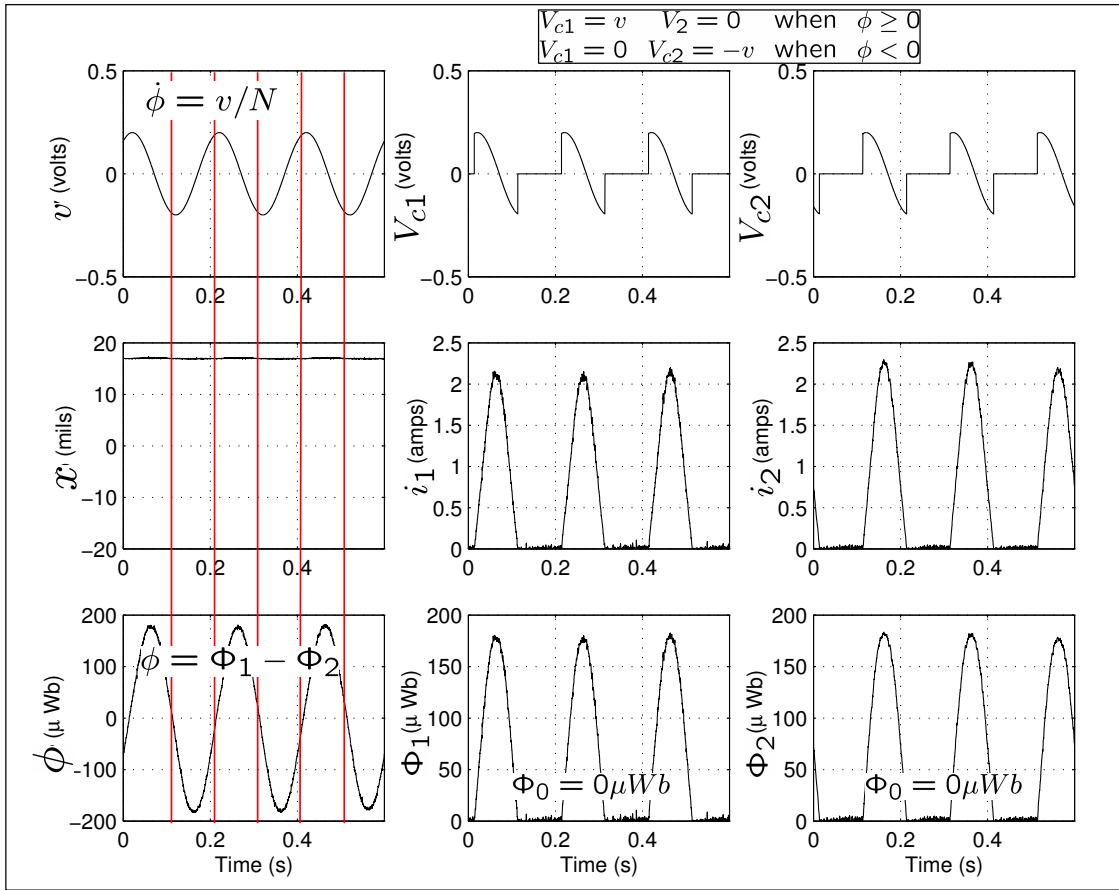


Figure 7. Open-loop GCFC implementation with sinusoidal control voltage v : $\Phi_0 = 0\mu\text{Wb}$. In this case, the GCFC corresponds to the CFC.

energy storage. Since the standard CFS constraint is a poor choice for low-loss AMB design, the GCFC is used. With the GCFC, one may operate the AMB with a large bias (to obtain some desired bearing stiffness and force slew-rate) or with a small bias (to achieve efficient AMB and FWB operation). In fact, using the GCFC, one may operate with zero bias-flux and still maintain controllability.

When using the GCFC, it is important to understand the effect of the bias value on the AMB performance measures (bearing stiffness, damping, force slew-rate, energy consumption, etc.) and evaluate the meaning of each measure according to the requirements of the AMB application. Furthermore, one may change the bias level to meet possibly time-varying performance requirements. For example, in an ESCMG application, one should reduce the bias for efficient energy storage. However, when the ESCMG is creating torque by gimballing the rotor spin axis, a larger bias may be required to regulate the rotor position. In addition, the challenges posed to the control design by the low bearing stiffness in ZB and LB must also be addressed. Specifically, when using voltage-mode amplifiers in ZB operation, one must preclude the existence singularities in the control law. An experimental comparison of the control laws introduced in Ref. [11] which implement the GCFC and address ZB and LB operation may be found in Refs. [17] and [23].

References

- ¹Dassaux, M., "The Industrial Applications of the Active Magnetic Bearings Technology," *Proceedings of the 2nd International Symposium on Magnetic Bearings*, July 1990, pp. 33–38, Tokyo, Japan.
- ²Knospe, C. R. and Fittro, R. L., "Control of a High Speed Milling Spindle via Mu-Synthesis," *Proc. of the 1997 IEEE Intl. Conf. on Contr. Apps.*, 1997, pp. 912–917, Hartford, CT.
- ³Darling, J. and Burrows, C. R., "The Control of Propeller-Induced Vibrations in Ship Transmission Shafts," *Proceedings of the 2nd International Symposium on Magnetic Bearings*, July 1990, pp. 169–174, Tokyo, Japan.
- ⁴Higuchi, T., Horikoshi, A., and Komori, T., "Development of an Actuator for Super Clean Rooms and Ultra High Vacua,"

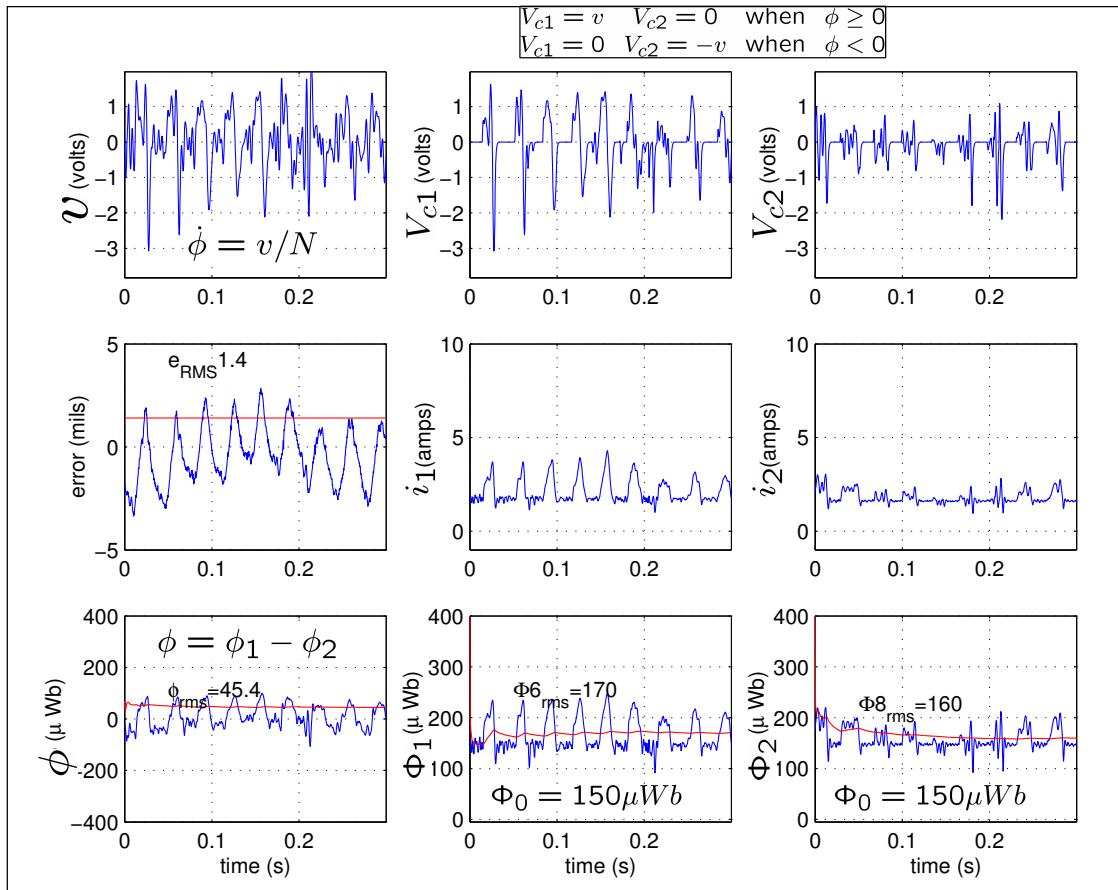


Figure 8. Closed-loop GCFC implementation with $\Phi_0 = 150\mu Wb$: Rotor is regulated against a periodic disturbance by a Passivity-based control law with gains $k_1 = 3$, $k_2 = 0.5$, and $\gamma = 0.5$.

Proceedings of the 2nd International Symposium on Magnetic Bearings, July 1990, pp. 115–122, Tokyo, Japan.

⁵Herbner, R., Beno, J., and Walls, A., “Flywheel Batteries Come Around Again,” *IEEE Spectrum*, April 2002, pp. 46–51.

⁶Fausz, J., “Control Issues in Simultaneous Attitude Control and Energy Storage,” Air Force Research Labs Summer Seminar Series on Structures and Control.

⁷McLallin, K. L., Soeder, J. F., and Jansen, R., “NASA Aerospace Flywheel IPACS Program,” Tech. rep., NASA Glenn Research Center, 2000.

⁸Wilson, B. C., Babuška, V., Potter, C., and Fausz, J. L., “Power System Design for a Spacecraft Simulator using Energy Storage Flywheels,” *3rd International Energy Conversion Engineering Conference*, AIAA, Aug. 2005, San Francisco, CA.

⁹Fausz, J. L., deBlonk, B. J., Babuška, V., and Fuentes, R. J., “FACETS Demonstration on AMPSS Facility, System Description Document- Release 1.4,” Tech. rep., Air Force Research Laboratory, Space Vehicles Directorate, Spacecraft Component Technologies (VSSV), May 2005.

¹⁰Li, L., “Linearizing Magnetic Bearing Actuators by Constant Current Sum, Constant Voltage Sum, and Constant Flux Sum,” *IEEE Trans. Magn.*, Vol. 35, No. 1, Jan. 1999, pp. 528–535.

¹¹Tsiotras, P. and Wilson, B. C., “Zero- and Low-Bias Control Designs for Active Magnetic Bearings,” *IEEE Trans. Contr. Syst. Technol.*, Vol. 11, No. 6, Nov. 2003, pp. 889–904.

¹²Charara, A., De Miras, J., and Caron, B., “Nonlinear Control of a Magnetic Levitation System Without Premagnetization,” *IEEE Trans. Contr. Syst. Technol.*, Vol. 4, No. 5, Sept. 1996, pp. 513–523.

¹³de Queiroz, M. S. and Dawson, D. M., “Nonlinear Control of Active Magnetic Bearings: A Backstepping Approach,” *IEEE Trans. Contr. Syst. Technol.*, Vol. 4, No. 5, Sept. 1996, pp. 545–552.

¹⁴Lévine, J., Lottin, J., and Ponstart, J. C., “A Nonlinear Approach to the Control of Magnetic Bearings,” *IEEE Trans. Contr. Syst. Technol.*, Vol. 4, No. 5, Sept. 1996, pp. 524–544.

¹⁵Wouterse, J. H., “Critical Torque and Speed of Eddy Current Brake with Widely Separated Soft Iron Poles,” *IEE Proceedings B (Electric Power Applications)*, Vol. 138, July 1991, pp. 153–158.

¹⁶Brown, D. and Hamilton III, E. P., *Electromechanical Energy Conversion*, MacMillian Publishing Company, New York, NY, 1984.

¹⁷Wilson, B. C. D., *Control Designs for Low-Loss Active Magnetic Bearings: Theory and Implementation*, Ph.D. thesis, Georgia Institute of Technology, May 2004.

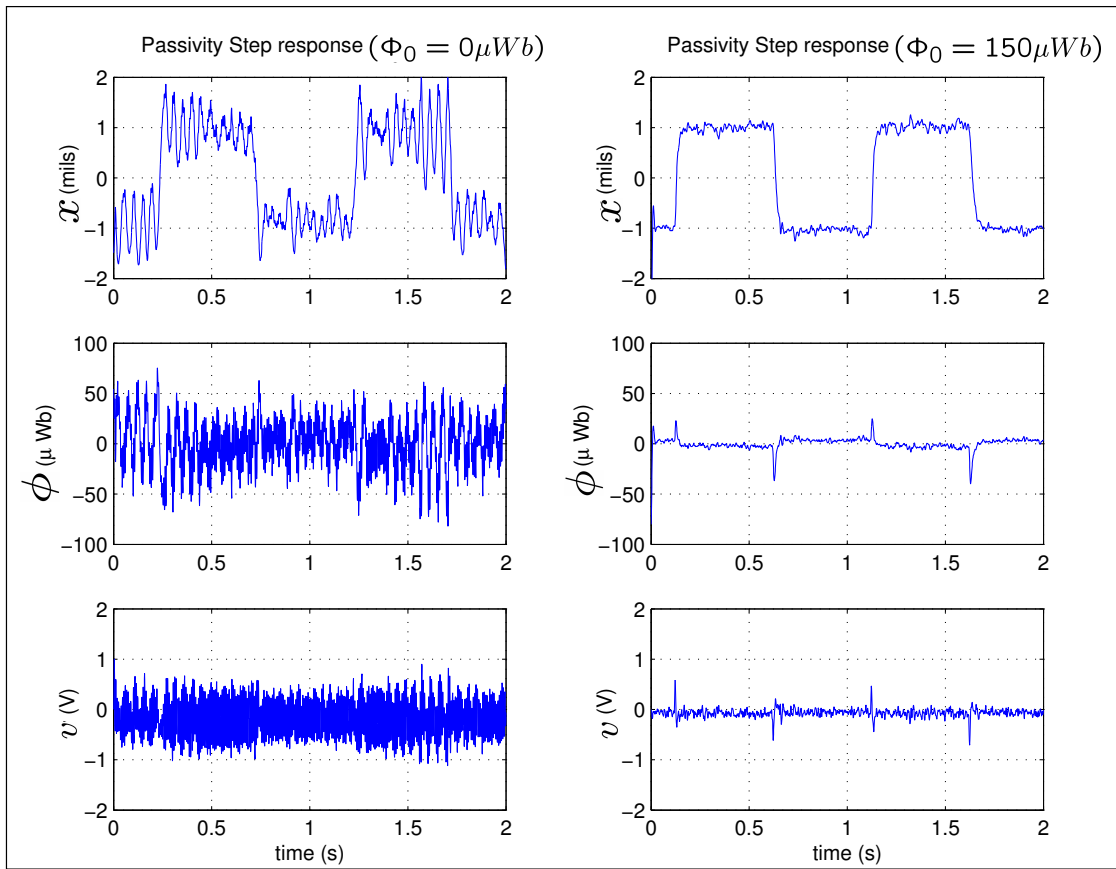


Figure 9. Step response of the rotor under Passivity-based control law with gains $k_1 = 3$, $k_2 = 0.5$, and $\gamma = 0.5$. Left and right columns are implemented with $\Phi_0 = 0\mu Wb$ and $\Phi_0 = 150\mu Wb$, respectively.

¹⁸Fitzgerald, A. E., Kingsley Jr., C., and Umans, S. D., *Electric Machinery*, McGraw-Hill, Inc., New York, NY, 5th ed., 1990.

¹⁹Knospe, C., "The Nonlinear Control Benchmark Experiment," *Proceedings of the American Control Conference*, 2000, pp. 2134–2138, Chicago, IL.

²⁰Maslen, E., Herman, P., Scott, M., and Humphris, R., "Practical Limits to the Performance of Magnetic Bearings: Peak Force, Slew Rate, and Displacement Sensitivity," *Transactions of the ASME Journal of Tribology*, Vol. 111, 1989, pp. 331–336.

²¹Bornstein, K., "Dynamic Load Capabilities of Active Electromagnetic Bearings," *Transactions of the ASME Journal of Tribology*, Vol. 113, 1991, pp. 598–603.

²²Tsiotras, P. and Arcaç, M., "Low-Bias Control of AMB Subject to Voltage Saturation: State-Feedback and Observer Designs," *Proc. of the 41st IEEE Conf. on Decision and Contr.*, Dec. 2002, pp. 2474–2479, Las Vegas, NV.

²³Wilson, B. C. D., Tsiotras, P., and Ferri-Heck, B. S., "Experimental Validation of Control Designs for Low-Loss Active Magnetic Bearings," *Proc. of the AIAA Guidance, Navigation, and Control Conf.*, aug 2005, to be published.